ACS APPLIED MATERIALS & INTERFACES

RESEARCH ARTICLE

www.acsami.org

Fabrication of Organic Field Effect Transistor by Directly Grown Poly(3 Hexylthiophene) Crystalline Nanowires on Carbon Nanotube Aligned Array Electrode

Biddut K. Sarker,[†,‡] Jianhua Liu,[†,§] Lei Zhai,[*,†,§] and Saiful I. Khondaker[*,†,‡,#]

[†]Nanoscience Technology Center, [‡]Department of Physics, [§]Department of Chemistry, and [#]School of Electrical Engineering and Computer Science, University of Central Florida, 12424 Research Parkway, suite 400, Orlando, Florida 32826, United States

Supporting Information

ABSTRACT: We fabricated organic field effect transistors (OFETs) by directly growing poly (3-hexylthiophne) (P3HT) crystalline nanowires on solution processed aligned array single walled carbon nanotubes (SWNT) interdigitated electrodes by exploiting strong $\pi-\pi$ interaction for both efficient charge injection and transport. We also compared the device properties of OFETs using SWNT electrodes with control OFETs of P3HT nanowires deposited on gold electrodes. Electron transport measurements on 28 devices showed that, compared to the OFETs with gold electrodes, the OFETs with SWNT electrodes have better mobility and better current on−off ratio with a maximum of 0.13 $cm^2/(V\,s)$ and 3.1×10^5, respectively. The improved device characteristics with SWNT electrodes were also demonstrated by the improved charge injection and the absence of short channel effect, which was dominant in gold electrode OFETs. The enhancement of the device performance can be attributed to the improved interfacial contact between SWNT electrodes and the crystalline P3HT nanowires as well as the improved morphology of P3HT due to one-dimensional crystalline nanowire structure.

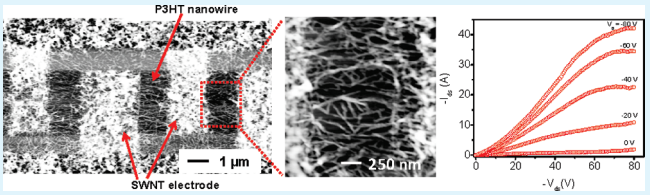

KEYWORDS: carbon nanotube electrodes, polymer nanowires, polythiophene, organic field effect transistor, solution processing, charge carrier injection

1. INTRODUCTION

The device performance of organic field effect transistors (OFET) is currently limited by the contact resistance between metal electrodes and organic semiconductors as well as the morphology of the semiconducting channel materials because of their highly anisotropic charge transport characteristics.[1−4] Contact resistance depends on the morphology of the interface, electrode work function, and dipole formation between electrodes and organic materials.[3,5−7] On the other hand, the nanoscale morphology of the organic semiconductors such as conjugated polymers is extremely sensitive to the polymer's molecular weights, the solvent to dissolve the polymer and cast films from, and the substrate treatments.[8,9] For example, the typical field effect charge mobility value for the most common solution processed conjugated polymer, poly(3-hexylthiophne) (P3HT), varies by several orders of magnitude depending upon the applied processing parameters.[4,5] Therefore, high performance OFETs can be fabricated by designing a new device architecture to improve the electrode/semiconductor contact for better charge injection and the morphology of the semiconductor for enhance charge mobility, where appropriate source and drain (S/D) electrode materials with excellent contact and highly ordered crystalline organic semiconducting materials hold the key.

Single-walled carbon nanotubes (SWNTs) are a promising candidate for electrode materials in OFETs because of their unique electrical properties.[10,11] The work function of SWNT thin films is in the range of 4.7−5.2 eV,[12] which is well-aligned with the HOMO (highest occupied molecular orbital) level of many conjugated polymers including P3HT.[1] In addition, the $\pi-\pi$ interaction between SWNTs and the conjugated polymers is expected to result in better charge injection. A few research groups have reported the fabrication of OFETs using individual SWNT,[13,14] randomly oriented SWNT network,[15−17] and SWNT/polymer composite film[18,19] as electrodes. In all of these studies, the organic materials were deposited by spin-coating, drop-casting, or by thermal evaporation, which resulted in poor morphology. Despite the conceptual advantages and attractive features of SWNTs as an electrode material, so far the performance of the OFET using SWNT electrodes did not demonstrate any improvement compared to that of conventional OFET fabricated with standard metal electrodes probably because of poorly defined crystalline structure of semiconductor materials.

One potential key step of improving the OFET device performance could be the direct growth of crystalline conjugated polymer such as P3HT nanowires on the SWNT electrodes to improve the electrode/semiconductor interface and the morphology of semiconductor. Compared to the OFETs from solution cast P3HT films, OFETs from crystalline P3HT nanostructures is expected to show improved mobility attributed to their increased

Received: January 4, 2011
Accepted: March 15, 2011
Published: March 15, 2011

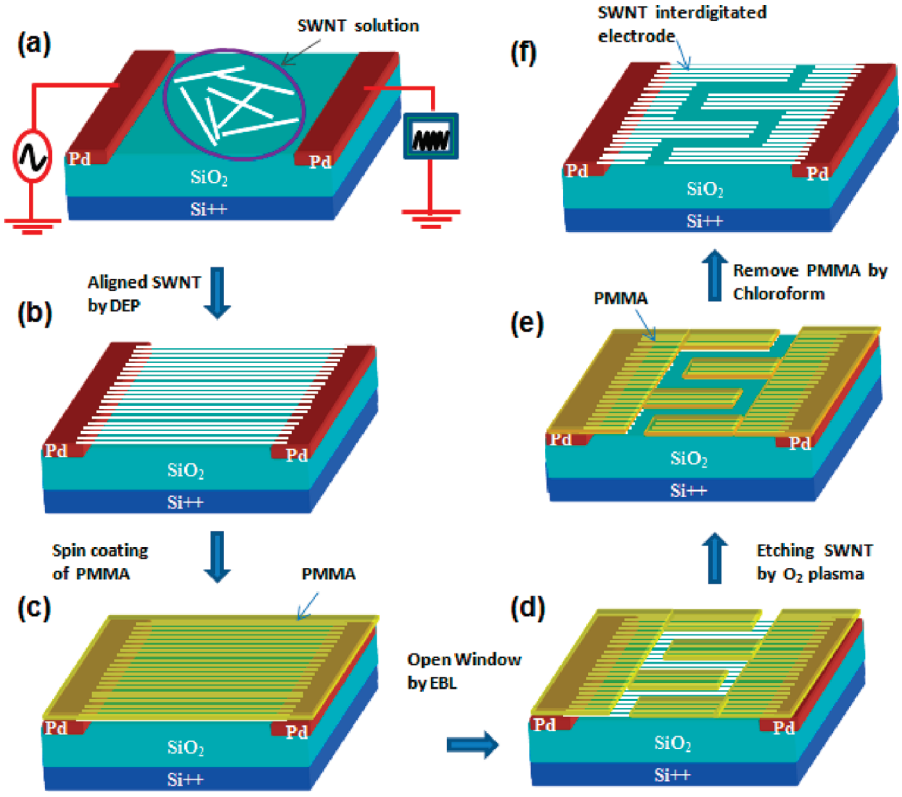

Figure 1. Schematics of the SWNT aligned array interdigitated electrode fabrication. (a, b) Aligning ultrahigh density SWNTs from high-quality SWNT aqueous solution via DEP between prefabricated palladium (Pd) patterns on Si/SiO_2 substrate, (c) spin-coating PMMA resist, (d) opening a window on the SWNTs array via EBL, (e) etching the exposed SWNTs by oxygen plasma to make SWNT electrode, and finally (f) removing PMMA using chloroform. Schematic shows only part of the electrode pattern.

interchain stacking with overlapped $\pi-\pi$ orbital and unique crystalline structure and morphology.[20−24] In addition, the surface treatments or other processing parameters will not have significant impact on the crystalline structures of P3HT since the ordered nanoscale morphology is developed during the growth process. In such devices, the strong $\pi-\pi$ interaction between SWNTs and the polymer nanowires will enhance the charge carrier injection from SWNT electrode to crystalline nanowires. In addition, the polymer nanowires will eliminate the crystal domain boundaries in thin films and improve the charge carrier transport through the channel along the one-dimensional supramolecular self-organized structures.[20]

In this work, we demonstrate a bottom-up approach to fabricate OFETs by growing P3HT crystalline nanowires on solution processed aligned array SWNT interdigitated electrodes which exploit strong $\pi-\pi$ interaction for both efficient charge injection and transport. Ultrahigh density SWNTs were aligned from their aqueous solutions via dielectrophoresis (DEP), while electron beam lithography (EBL) and oxygen plasma etching technique was used to define the SWNT electrode pattern. The P3HT crystalline nanowires were directly grown from SWNT surface to connect the SWNT electrodes. For comparison of device properties, control OFETs of P3HT nanowires deposited on gold electrodes were also fabricated. Electron transport measurements on 28 devices showed that, compared to the OFETs with gold electrodes, the OFETs with SWNT electrodes have shown better mobility and better current on−off ratio with a maximum of 0.13 $cm^2/(V\,s)$ and 3.1×10^5 respectively. The improved device characteristics with SWNT electrodes were also demonstrated by the improved charge injection and the absence of short channel effect which was dominant in gold electrode OFETs. Such remarkable enhancement of the device performance as high mobility, high current on−off ratio, absence of short channel effect and better charge carrier injection can be attributed to the improved contact via strong $\pi-\pi$ interaction between SWNT electrodes and the crystalline P3HT nanowires as well as the improved morphology of P3HT due to one-dimensional crystalline structure.

2. EXPERIMENTAL SECTION

Fabrication of SWNT Electrodes. The step-by-step nanotube electrodes fabrication procedures are illustrated in Figure 1. At first, palladium (Pd) patterns were fabricated by EBL followed by thermal evaporation of 30 nm Pd and standard lift-off. SWNTs were aligned between the Pd patterns using DEP. DEP has been shown to assemble 2D, 1D, and 0D nanomaterials at the selected position of the circuit for device applications.[25−29] Highly purified, stable, and surfactant-free SWNT aqueous solution was obtained from Brewer Science Inc.[30] and was diluted by six times in DI water. A 3 μL drop of the solution was placed on the Pd patterns and an ac voltage of 5 Vp-p at 300 kHz was applied between the Pd patterns for 30 s (Figure 1a). The ac voltage creates a time averaged dielectrophoretic force between Pd electrode patterns and aligns the SWNTs (see details in the Supporting Information, Figure S1). After SWNT alignment, PMMA was spin coated on the samples at 4000 rpm for 60 s followed by baking at 180 °C for 15 min on a hot plate (Figure 1c). A precise window of interdigitated electrode pattern was opened by EBL writing and developing in a mixture of MIBK

and IPA (Figure 1d). The EBL was done by Zeiss Ultra-55 SEM combined with Nabity pattern generator. To etch the exposed SWNT array through the open window, the samples were put in the oxygen plasma cleaner and were etched for 10 min (Figure 1e). Finally, devices were kept into the chloroform for 12 h and rinse with acetone, IPA, ethanol and DI water to remove the remaining PMMA (Figure 1f). For control experiment, gold interdigitated electrodes were also fabricated with the same geometry of SWNT electrodes by EBL and thermal deposition of gold and standard lift off. All of the OFET devices in this experiment had channel length (L) of 1 μm and total channel width (W) of 40 μm.

Growth of P3HT Nanowires on SWNT Electrodes. P3HT and anisole were purchased from Rieke Metals, Inc. and Acros Organics (New Jersey, USA) respectively and used as received. In this experiment, no additional surface treatment such as octadecyltrichlorosilane (OTS) or hexamethyldisilazane (HMDS) was performed on SiO_2 surface. P3HT powder was dissolved in anisole with a concentration of 0.25 mg/mL at 90 °C in a glass vial. One chip of SWNT electrode was then immersed inside the P3HT solution, which was cooled down to room temperature at a rate ~20 °C/h and kept 12 h for P3HT crystallization.

Characterization of Devices. Tapping mode atomic force microscopy (AFM) images were acquired by Dimension 3100 AFM (Veeco). The scanning electron microscopy (SEM) images were taken using Zeiss Ultra −55 SEM with an accelerating voltage 1 kV. Raman spectroscopy was performed using a Renishaw InVia Raman microscope comprised of a laser (532 nm line of solid Si laser), a single spectrograph fitted with holographic notch filters, and an optical microscope (a Leica microscope with a motorized XYZ stage) rigidly mounted and optically coupled to the spectrograph. The spectrometer was calibrated with a Si standard using a Si band position at 520.3 cm^{-1}. The electrical transport measurements of SWNT array were carried out by DL instruments 1211 current preamplifier and a Keithley 2400 source meter interfaced with LabView program. The OFET characteristics were measured using Hewlett-Packed (HP) 4145B semiconductor parametric analyzer connected to a probe station inside an enclosed glovebox system filled with nitrogen gas.

3. RESULTS AND DISCUSSION

Figure 2a shows a SEM image of a part of the SWNT aligned array assembled via DEP. By controlling the concentration of the SWNT in the solution, we can control the linear density and sheet resistance of the aligned array (see Figure S1 in the Supporting Information). Details of the SWNT alignment and characterization can be found in our recent report.[31] The current (I_{ds}) − voltage (V_{ds}) characteristic of this array is shown in Figure 2b (red solid line) from which a resistance of about 400 Ω and a sheet resistance of 2 KΩ/□ were calculated. In this report, all the electrodes were fabricated from densely packed aligned array so that the resistances of the arrays are low (<500 Ω). In addition, our SWNT aligned array does not show any gate voltage dependence (see Figure S2 in the Supporting Information) indicating that the aligned array behaves as a metallic system. The low resistance and metallic behavior of the SWNT array makes them ideal materials for OFET electrodes. The interdigitated electrode pattern was then defined using EBL and oxygen plasma etching. Figure 2c shows a SEM image of a part of the fabricated SWNT electrode with well-defined channel length L = 1 μm. For channel width, we considered all contributions including channel between parallel SWNT fingers as well as channel between the SWNT fingers and SWNT base. The total channel width were W = 40 μm giving a W/L ratio of 40. (see Supporting Information for SEM image of one complete electrode and width calculation). After the oxygen plasma

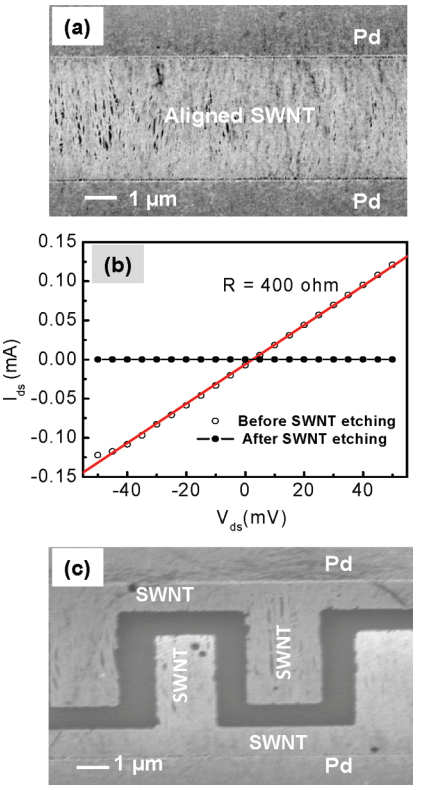

Figure 2. (a) Scanning electron microscopy (SEM) image of a part of densely aligned SWNT array assembled via dielectrophoresis. (b) Drain current (I_{ds}) as a function of bias voltage (V_{ds}) with zero gate bias before (red line) and after (black line) SWNT etching. (c) SEM image of a part of SWNT interdigital electrode.

etching, we measured the I_{ds} −V_{ds} again and found the current to be in the pico ampere range (leakage current, black line in Figure 2b) suggesting that no SWNT was left in the channel. The interdigitated electrode patterns were chosen in this work because the interdigitated patterns provide maximum surface area for the growth of P3HT nanowires. In addition, the interdigitated electrodes can increase the output current by increasing the channel width while keeping the device size small.

The unique feature of our OFET fabrication using SWNT electrodes is the direct growth of crystalline P3HT nanowires in between SWNT interdigitated electrodes by a bottom up approach.[23] When the chip containing SWNT electrodes was immersed into the hot P3HT solution and allowed to cool down to room temperature, it induced the crystallization of P3HT in the solution to form 1D nanowire-like crystals.[24] Because SWNTs function as the nucleation cores for P3HT through the $\pi-\pi$ interactions, P3HT nanowires grow from the surface of SWNTs,[23] generating the interconnections (P3HT nanowire network) among the SWNTs in the electrodes. The AFM images (Figure 3a,b) clearly show that the P3HT nanowires connect SWNT source and drain interdigitated electrodes. Because P3HT nucleates on all the SWNTs, the brighter part represents SWNT electrodes, whereas the relatively darker part represents the channel. For a control experiment, individually dispersed SWNTs (not in the electrode form) were also placed in the P3HT solution under the same condition. The transmission electron microscopy (TEM) image of this growth (Figure 3c, and Figure S4 in the Supporting Information) shows that the P3HT

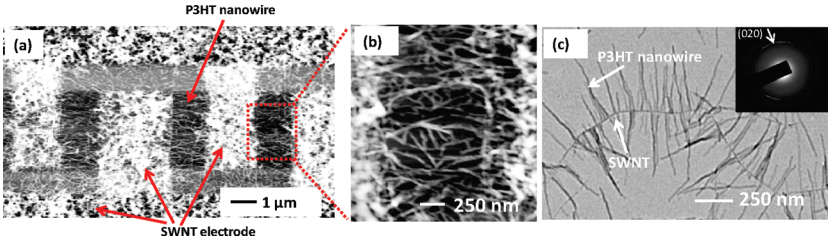

Figure 3. (a) Atomic force microscopy (AFM) image of P3HT nanowire growth on SWNT interdigitated electrodes (This image represents only a part of the device). (b) High-magnification image of image a. (c) Transmission electron microscopy (TEM) images of P3HT nanowires growth on SWNT surface. Inset in c: Selected area electron diffraction (SAED) pattern of the nanowires.

nanowires grow from nanotube surfaces and no free P3HT nanowires were observed in the solution. The obtained selected area electron diffraction (SAED) patterns of these nanowires (inset in Figure 3c) show the (020) reflection (d = 0.38 ± 0.01 nm), confirming that the polymer chains were well-stacked perpendicularly to the nanowire long axis (direction of $\pi-\pi$ interaction). In addition, Raman spectra of SWNTs and SWNTs with P3HT nanowires (see Figure S5 in the Supporting Information) indicates the molecular level interaction between SWNT and P3HT, suggesting good contact between two materials. Gold interdigitated electrodes (see Figure S6a in the Supporting Information) with the same architecture as SWNT electrodes were also immersed into the P3HT hot anisole solutions to check the growth of P3HT nanowires on the gold electrodes. Since there is no interaction between gold electrodes and P3HT, it is not surprising to find out that P3HT form nanowires in the cooled solution and deposit randomly on the gold electrodes (see Figure S6b in the Supporting Information). The gold electrode OFET with similar P3HT coverage density as the SWNT electrode OFET was fabricated for comparison of device characteristics. A total of 14 OFET devices with SWNT electrodes and 14 OFET devices with gold electrodes were studied.

The output characteristics ($I_{ds} - V_{ds}$) of a representative OFET device with SWNT electrodes shows excellent gate modulation along with current saturation (Figure 4a). The transfer characteristic ($I_{ds} - V_g$) of the same device at a fixed V_{ds} = −60 V (Figure 4b) shows the current varies over 5 orders of magnitude (I_{on}/I_{off} = 3.1 × 10^5) with a threshold voltage (V_T) of −20 V. The saturation mobility (μ_{sat})and linear mobility (μ_{lin}) of the OFET devices were calculated using the standard formula $\mu_{sat} = I_{ds,sat}(2L/WC_i)(1/(V_g-V_T)^2)$ and $\mu_{lin} = (L/WC_iV_{ds})(dI_{ds}/dV_g)$, respectively; where C_i is the capacitance per unit area of the gate insulator (13.8 nF/cm^2).[1] The μ_{sat} and μ_{lin} of this device were 0.065 cm^2/(V s) and 0.04 cm^2/(V s) respectively. From the AFM images, it is estimated that the OFET channel is ∼50% covered by P3HT nanowires, giving an effective channel width of 20 μm. Using this effective channel width, the calculated effective saturation and linear mobility were 0.13 and 0.08 cm^2/(V s), respectively. All 14 studied SWNT electrode OFET devices have shown similar saturation behavior with effective μ_{sat} varying from 0.03 to 0.13 cm^2/(V s) (average μ_{sat} = 0.07 ± 0.03 cm^2/(V s)), with corresponding I_{on}/I_{off} varying from 7.1 × 10^3 to 3.1 × 10^5. The maximum mobility (0.13 cm^2/(V s)) of the fabricated devices is 1 order of magnitude higher than the previous reported values of P3HT film OFET spin coated on the carbon nanotube electrode.[16] This is rather impressive considering the fact that no surface treatment was performed on our devices. The reason for the improved mobility of our P3HT nanowire OFETs with SWNT electrode is

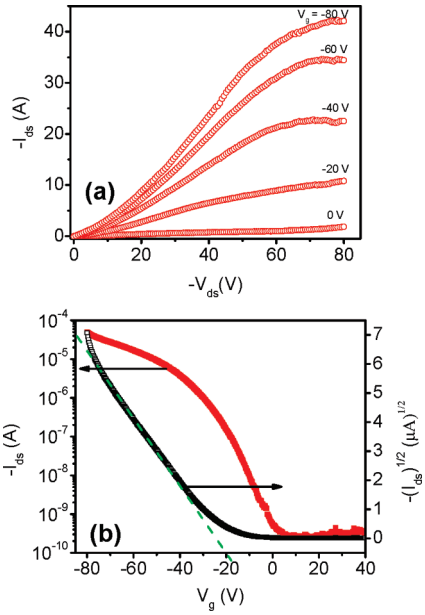

Figure 4. (a) Output characteristics of a representative P3HT-nanowire OFET with SWNT interdigitated electrodes with dimension of L = 1 μm and W = 40 μm, fabricated on a Si/SiO_2 substrate with an oxide thickness of 250 nm. (b) Transfer curve of the same OFET showing the current on−off ratio (I_{on}/I_{off}) to be 3.1 × 10^5.

because of the highly ordered crystalline nanowire form of the P3HT, which provides better charge transport pathways, as well as direct growth of these nanowires on the surface of nanotube electrode, which provides better interface.

We have also measured control P3HT nanowire OFETs with gold interdigitated electrodes. Output characteristics of one of our best P3HT-nanowire OFET with gold interdigitated electrode is shown in Figure 5a. The output current shows parabolic behavior with voltage without showing any saturation, typical of space charge limited conduction and has been commonly observed in short channel metal electrode OFETs[32−34]. The parabolic behavior indicates the presence of an interfacial barrier at P3HT/gold interface. The transfer characteristics of the same device is presented in Figure 5b measured in the linear regime (V_{ds} = −40 V) which show a current on−off ratio 2.6 × 10^4. Since the output curve is not saturated, we only calculated effective linear mobility μ_{lin}= 0.045 cm^2/(V s) for this device by considering ∼50% coverage (please see Figure S6 in the Supporting Information). Of the 14 devices that we measured using gold electrodes, majority of them showed short channel behavior with μ_{lin} varying from 0.001 to 0.045 cm^2/(Vs)

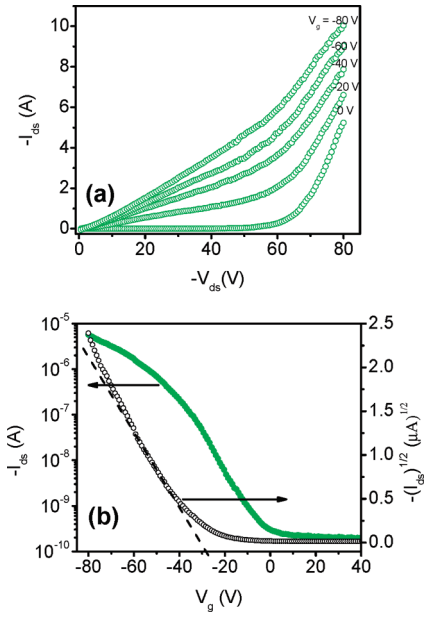

Figure 5. (a) Output characteristics of the best P3HT-nanowire OFET device with gold interdigitated electrodes. (b) Transfer curve of the same device.

(average μ_{lin} = 0.02 ± 0.01 cm^2/(V s)). The corresponding I_{on}/I_{off} of the devices vary from 10 to 3 × 10^4. Figure S7 (see the Supporting Information) shows a summary of the device characteristics for all SWNT electrode OFETs and gold electrode OFETs. From here, we see that although SWNT electrode OFETs have shown an improved and more consistent device performance, gold electrode OFETs show a larger variation in performance. This again shows that how the short channel effect dominates gold electrode OFETs.

It is well-known that when L is less than 10 times the oxide thickness (t_{ox}), the device performance is dominated by the short channel effect[1,3,32−34] which manifests as parabolic behavior of output current without saturation and high off current. Therefore, the observed short channel effect in the gold electrode OFET (t_{ox} = 250 nm, L = 1 μm) is as-expected. Because I_{on}/I_{off} depends on L according to $I_{on}/I_{off} = (4C_i/9t_{ox}\varepsilon\varepsilon_0)L^2$; where, ε_0 is the vacuum permittivity and ε is the dielectric constant of channel insulator,[35] it is very difficult to achieve perfect transistor behavior and high I_{on}/I_{off} in a short channel OFET. It is, however, interesting to observe that the OFET with SWNT electrodes (same L and t_{ox}) did not show any short channel effect, instead it showed perfect saturation with high I_{on}/I_{off} (Figure 4a,b). Such observation is significant because the short channel effect is a major bottleneck in reducing the device size for high performance OFETs. It is believed that the better contact between P3HT nanowires and SWNT electrodes as well as the improved morphology of the channel material because of their crystalline nanowire structures eliminated the short channel effect. To investigate the role of P3HT/SWNT electrode contact in the charge injection into the P3HT nanowires, we plotted low bias output characteristics with zero and −60 V gate voltage for both SWNT and gold electrodes (Figure 6a and 6b). From these curves, it is clear that the OFET with SWNT electrodes provides more output current than that with gold electrode under the same applied voltage.

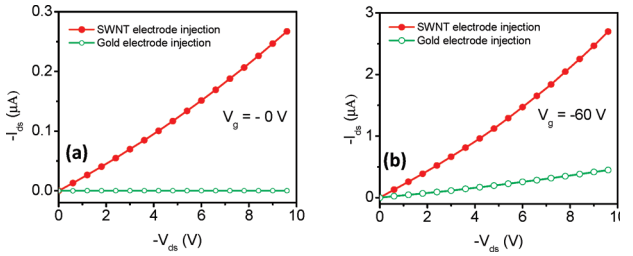

Figure 6. Comparison of charge injection from SWNT electrode and gold electrode into the P3HT nanowires at low bias (V_{ds} = −10 V) and with a gate voltage (a) V_g = 0 V and (b) V_g = −60 V. Both curves show that compared to a gold electrode, SWNT electrodes provides a higher drain current because of a better charge injection.

The remarkable improvement of the device performance including high mobility, high current on−off ratio, the absence of short channel effect, and better charge carrier injection can be attributed to the improved contact between aligned array SWNT electrodes with the crystalline P3HT nanowires as well as improved morphology of P3HT. The SWNTs and P3HTs share the same conjugated carbon hexagonal ring structure, and strong π−π interaction exists between P3HT nanowires and SWNTs. This makes excellent interfacial contact between P3HT nanowires and SWNTs and leads to efficient charge carrier injection from SWNT electrodes to P3HT nanowires. The highly ordered P3HT nanowires reduce the gain boundaries in the channel, provide the high current conducting path between nanotube S/D electrodes, and enhanced the hole mobility in the device.[4,5,20−22]

4. CONCLUSIONS

In summary, we demonstrated new device architecture for high-performance OFET fabrication using the direct growth of crystalline P3HT nanowires on SWNT interdigitated electrodes. Compared to the OFETs with metal electrodes, the devices with SWNT electrodes have shown consistently high mobility and high current on−off ratio with a maximum of 0.13 cm^2/(V s) and 3.1 × 10^5, respectively. The improved device characteristics were also demonstrated by the absence of short channel effect which was dominant in gold electrode OFETs. Such remarkable improvement of the device performance as high mobility, high current on−off ratio, absence of short channel effect, and better charge carrier injection can be attributed to the improved contact via strong π−π interaction SWNT electrodes with the crystalline P3HT nanowires as well as the improved morphology of P3HT due to one-dimensional crystalline structure. Our results presented here will have significant impact on the development of high-performance organic electronic devices.

■ ASSOCIATED CONTENT

Supporting Information. (1) Alignment of carbon nanotubes by dielectrophoresis (DEP). (2) Gate voltage dependence of the SWNT aligned array. (3) SEM image of a full SWNT electrode. (4) Crystalline growth of P3HT nanowires on carbon nanotubes. (5) Raman spectroscopic studies of SWNT with P3HT Nanowires. (6) OFET fabrication with gold interdigitated electrode. (7) Device statistics of OFETs with SWNT and gold electrodes. This material is available free of charge via Internet at http://pubs.acs.org.

AUTHOR INFORMATION

Corresponding Author
*E-mail: lzhai@mail.ucf.edu (L.Z.); saiful@mail.ucf.edu (S.I.K.).

ACKNOWLEDGMENT

This work is partially supported by U.S. National Science Foundation under Grant ECCS 0801924, 1102228, and DMR 0746499. The help from Dr. Nina Orlovskaya (Raman spectroscopy) is greatly appreciated.

REFERENCES

(1) Zaumseil, J.; Sirringhaus, H. *Chem. Rev.* **2007**, *107*, 1296–1323.
(2) Virkar, A. A.; Mannsfeld, S.; Bao, Z.; Stingelin, N. *Adv. Mater.* **2010**, *22*, 3857–3885.
(3) Bürgi, L.; Richards, T. J.; Friend, R. H.; Sirringhaus, H. *J. Appl. Phys.* **2003**, *94*, 6129–6137.
(4) Surin, M; Leclère, Ph.; Lazzaroni, R. *J. Appl. Phys.* **2006**, *100*, 033712.
(5) Singh, K. A.; Sauvé, G; Zhang, R.; Kowalewski, T.; McCullough, R. D.; Porter, L. M. *Appl. Phys. Lett.* **2008**, *92*, 263303.
(6) Koch, N.; Kahn, A; Ghijsen, J.; Pireaux, J.-J.; Schwartz, J.; R. L. Johnson, R. L.; Elschner, A. *Appl. Phys. Lett.* **2003**, *82*, 70–72.
(7) Hill, I. G.; Rajagopal, A.; Kahn, A; Hu, Y. *Appl. Phys. Lett.* **1998**, *73*, 662–664.
(8) Kline, R.; J.; McGehee, M. D.; Kadnikova, E. N.; Liu, J.; Fre'chet, J. M. J.; Toney, M. F. *Macromolecules* **2005**, *38*, 3312–3319.
(9) Kobayashi, S.; Nishikawa, T.; Takenobu, T.; Mori, S.; Shimoda, T.; Mitani, T.; Shimotani, H.; Yoshimoto, N.; Ogawa, S.; Iwasa, Y. *Nat. Mater.* **2004**, *3*, 317–322.
(10) Guo, X.; Small, J. P.; Klare, J. E.; Wang, Y.; Purewal, M. S.; Tam, I. W.; Hong, B. H.; Caldwell, R.; Huang, L.; O'Brien, S.; Yan, J.; Breslow, R.; Wind, S. J.; Hone, J.; Kim, P.; Nuckoll, C. *Science* **2006**, *311*, 356–359.
(11) Qi, P.; Javey, A.; Rolandi, M.; Wang, Q.; Yenilmez, E.; Dai, H. *J. Am. Chem. Soc.* **2004**, *126*, 11774–11775.
(12) Hu, L.; Hecht, D. S.; Gruner, G. *Chem. Rev.* **2010**, *110*, 5790–5844.
(13) Aguirre, C. M.; Ternon, C.; Paillet, M.; Desjardins, P.; Martel, R. *Nano Lett.* **2009**, *9*, 1457–1461.
(14) Tsukagoshi, K.; Yagi, I.; Aoyagi, Y. *Appl. Phys. Lett.* **2004**, *85*, 1021–1023.
(15) Chang, C.-H.; Chien, C.-H.; Yang, J.-Y. *Appl. Phys. Lett.* **2007**, *91*, 083502.
(16) Southard, A.; Sangwan, V.; Cheng, J.; Williams, E. D.; Fuhrer, M. S. *Org. Electron.* **2009**, *10*, 1556–1561.
(17) Zhang, Y. Y.; Shi, Y.; Chen, F.; Mhaisalkar, S. G.; Li, L.-J.; Ong B. S. Wu, Y. *Appl. Phys. Lett.* **2007**, *91*, 223512.
(18) Hellstrom, S. L.; Jin, R. Z.; Stoltenberg, R. M.; Bao, Z. *Adv. Mater.* **2010**, *22*, 4204–4208.
(19) Lefenfeld, M.; Blanchet, G.; Rogers, J. A. *Adv. Mater.* **2003**, *15*, 1188–1191.
(20) Kim, D. H.; Jang, Y.; Park, Y. D.; Cho, K. *J. Phys. Chem. B* **2006**, *110*, 15763–15768.
(21) Lan, Y.-K.; Huang, C.-I. *J. Phys. Chem. B* **2009**, *113*, 14555–14564.
(22) Arif, M.; Liu, J.; Zhai, L.; Khondaker, S. I. *Appl. Phys. Lett.* **2010**, *96*, 243304.
(23) Liu, J.; Zou, J.; Zhai, L. *Macromol. Rapid Commun.* **2009**, *30*, 1387–1391.
(24) Liu, J.; Arif, M.; Zou, J.; Khondaker, S. I.; Zhai, L. *Macromolecules* **2009**, *42*, 9390–9393.
(25) Joung, D.; Chunder, A.; Zhai, L.; Khondaker, S. I. *Nanotechnology* **2010**, *21*, 165202.
(26) Stokes, P.; Khondaker, S. I. *Nanotechnology* **2008**, *17*, 175202.
(27) Stokes, P.; Khondaker, S. I. *Appl. Phys. Lett.* **2010**, *96*, 083110.
(28) Khondaker., S. I. *IEE Proc. Circuits, Devices Syst.* **2004**, *151*, 457.
(29) Khondaker, S. I.; Luo, K.; Yao., Z. *Nanotechnology* **2010**, *21*, 095204.
(30) http://www.brewerscience.com/products/carbon-nanotube/
(31) Shekhar S.; Stokes P.; Khondaker, S. I. *ACS Nano*, **2011**, *5*, 1739.
(32) Collet, J.; Tharaud, O.; Chapoton, A; Vuillaume., D *Appl. Phys. Lett.* **2000**, *76*, 1941.
(33) Wang, J. Z.; Zheng, Z. H.; Sirringhaus, H. *Appl. Phys. Lett.* **2006**, *89*, 083513.
(34) Tsukagoshi, K.; Fujimori, F.; Minari, T.; Miyadera, T; Hamano, T.; Aoyagi, Y. *Appl. Phys. Lett.* **2007**, *91*, 113508.
(35) Koehler, M.; Biaggio, I. *Phys. Rev. B.* **2004**, *70*, 045314.